EDGE ARTICLE

Check for updates

Feshbach resonances in the F + CHD₃ → HF + CD₃ reaction†

Shu Liu, [ID] *[ab] Jun Chen, [ID] [c] Xiaoren Zhang[a] and Dong H. Zhang [ID] *[ab]

The signature of dynamics resonances was observed in the benchmark polyatomic F + CH₄/CHD₃ reactions more than a decade ago; however, the dynamical origin of the resonances is still not clear due to the lack of reliable quantum dynamics studies on accurate potential energy surfaces. Here, we report a six-dimensional state-to-state quantum dynamics study on the F + CHD₃ → HF + CD₃ reaction on a highly accurate potential energy surface. Pronounced oscillatory structures are observed in the total and product rovibrational-state-resolved reaction probabilities. Detailed analysis reveals that these oscillating features originate from the Feshbach resonance states trapped in the peculiar well on the HF(v' = 3)–CD₃ vibrationally adiabatic potential caused by HF chemical bond softening. Most of the resonance structures on the reaction probabilities are washed out in the well converged integral cross sections (ICS), leaving only one distinct peak at low collision energy. The calculated HF vibrational state-resolved ICS for CD₃(v = 0) agrees quantitatively with the experimental results, especially the branching ratio, but the theoretical CD₃ umbrella vibration state distribution is found to be much hotter than the experiment.

Over the past decades, a clear physical picture of the reaction resonances in the F + H₂/HD/H₂O/HOD/NH₃ reactions has been established through close interaction between high-resolution crossed-molecular beams or transition-state spectroscopy experiments and quantum dynamics calculations on highly accurate potential energy surfaces (PESs).[1–10] All these hydrogen abstraction reactions involving a F atom possess similar dynamical resonances trapped by the HF vibrational excited adiabatic potential wells in the post-barrier region.

Like the F + H₂/H₂O/NH₃ systems, the F + CH₄ → HF + CH₃ reaction is another benchmark system for highly exothermic hydrogen abstraction reactions with a low and early barrier. It has a bent transition-state geometry, a shallow van der Waals (vdW) well in the entrance channel and a deeper vdW well in the exit channel, both with linear configurations. The reaction plays an important role in atmospheric chemistry and can yield a highly inverted HF(v') vibrational distribution, which shows great potential in the production of chemical lasers.[11–13] Liu and coworkers reported the first experimental signature of reactive resonances in a polyatomic reaction in the F + CH₄/CHD₃ reaction.[14–17] In the F + CHD₃(v = 0) reaction, they observed a step-like feature in the excitation function of the CD₃(v = 0) + HF

channel at low collision energies,[15] which echoes the resonance fingerprints in the integral cross sections (ICS) of the F + HD → HF + D reaction.[18,19] Furthermore, the excitation function of the CHD₂(v = 0) + DF channel displays a 'kink' in shape at about the same energy.[15] The differential cross-sections (DCS) of the two isotopic channels both show a near-threshold ridge and oscillatory forward–backward peaking, which also provide strong support for reactive resonances.[16] The cross-sections of the bending-excited reaction F + CHD₃(v_b = 1) also show peak features for the CD₃(v_2 = 0,1) + HF(v' = 3) channels.[17] In addition, they observed anticorrelation in the vibrational states of the coincident product pairs of CD₃(v_2) and DF(v') in the F + CD₄ reaction.[20–22]

Theoretically, great efforts have been devoted to the construction of an accurate potential energy surface (PES) for the F + CH₄ system.[23–28] In 2009, Czakó *et al.* constructed a full-dimensional PES with permutational invariant polynomials (PIP) method called CSBB PES,[29] and subsequently improved the PES by including the spin–orbit (SO) coupling term of the F atom.[30] In 2014, Westermann *et al.*[31,32] constructed the coupled diabatic WEM PESs for the entrance channel region containing vibronic as well as SO coupling effects and connected the lowest adiabatic one with the CSBB PES in the interaction region to acquire a global adiabatic PES called PWEM PES. Later, they constructed the globally defined coupled diabatic PESs[33] by using the same set of diabatic electronic states in the transition state region and all four exit channels. In 2018, our group constructed a global PES for the system using a neural network (NN) fitting method based on 99 000 UCCSD(T)-F12a/aug-cc-pVTZ *ab initio* energies.[34] Correction terms considering the

[a]*State Key Laboratory of Molecular Reaction Dynamics, Dalian Institute of Chemical Physics, Chinese Academy of Sciences, Dalian, Liaoning 116023, China. E-mail: liushu1985@dicp.ac.cn; zhangdh@dicp.ac.cn*

[b]*University of Chinese Academy of Sciences, Beijing 100049, China*

[c]*State Key Laboratory of Structure Chemistry, Fujian Institute of Research on the Structure of Matter, Chinese Academy of Sciences, Fuzhou, Fujian 350002, China*

† Electronic supplementary information (ESI) available. See DOI: https://doi.org/10.1039/d3sc02629a

influence of a larger basis set as well as spin–orbit couplings were further implemented with a hierarchical scheme. With a fitting error of ~4.87 meV for energies within 2.5 eV, our NN PES is substantially more accurate than the previous ones.

The theoretical evidence for reactive resonances in the $F + CH_4$ reaction was first reported by Nyman et al. through the oscillations in the cumulative reaction probabilities (CRP) and the dramatic change of DCS with collision energy[35] by using the time-independent three-dimensional rotating line umbrella (RLU) quantum scattering model. Wang showed the resonance features in the initial-state-selected total reaction probabilities and the ICS calculated by using the four-degree-of-freedom quantum dynamics approach on the CSBB PES.[36] Westermann et al. found resonances trapped in the entrance channel vdW well of the $F + CH_4$ system[32] via the transition-state spectra calculated using the full-dimensional (12D) multi-configurational time-dependent Hartree (MCTDH) approach on the WEM PESs. For the $F + CHD_3$ reaction, von Horsten and Clary studied the reactive resonances using a two-dimensional model, which only described the bond breaking and bond forming explicitly. The final state resolved ICS for both reaction channels showed qualitative agreement with experimental results, although discrepancies remained in the branching ratios. They attributed the low energy peaks in the CRP to quasi-bound states with a quantum number $v' = 3$ of the H–F stretch mode, and $v' = 4$ of the D–F stretch mode in the product region.[37] Qi et al. performed eight-dimensional (8D) wave packet dynamics calculations[38] on the PWEM PES, and Zhao et al. performed seven-dimensional (7D) non-adiabatic wave packet dynamics calculations[39] on the global vibronically and SO-coupled diabatic PESs for the $F + CHD_3$ reaction. They both reported fast-oscillating structures on the total reaction probabilities at low collision energies, but attributed them to the resonances in the pre-reaction vdW well. Therefore, the origin of the resonances in the reaction is still not clear.

Here, we report six-dimensional (6D) state-to-state quantum dynamics studies of the $F + CHD_3 \rightarrow HF + CD_3$ reaction on the NN PES. Pronounced oscillatory structures are observed in the total reaction probabilities, in particular at collision energies below 0.05 eV. Detailed analysis reveals that these oscillating features originate from the Feshbach resonance states trapped in the peculiar well on the $HF(v' = 3)$–CD_3 vibrational adiabatic potential (VAP) caused by HF bond softening, mainly producing $HF(v' = 2)$. The calculated vibrational state-specific excitation functions of $HF(v') + CD_3(v = 0)$ are in good agreement with the experimental results. However, the theoretical CD_3 umbrella vibration state distribution is found to be much hotter than the experiment.

The reduced dimensional model employed in the time-dependent wave packet (TDWP) calculations here was the free-torsion seven-dimensional (FT-7D) model we proposed for the $X + YCZ_3 \rightarrow XY + CZ_3$ reaction in 2013, by assuming that the CZ_3 group can rotate freely with respect to its C_{3v} symmetry axis.[40] This is an additional approximation introduced to the original eight-dimensional (8D) model of Palma and Clary with the nonreacting CZ_3 group constrained in the C_{3v} symmetry[41] to reduce computational costs. With the bond length of CD fixed at its equilibrium value in the reactant (2.06 bohr) because it

essentially does not change during the reaction, the number of degrees of freedom included in the calculation was reduced to six. We used the multiple-step reactant-product decoupling (MRPD) method[42–44] to obtain the state-to-state information. We carried out state-to-state calculations for the total angular momentum $J_{tot} = 0, 10, 15, 20, 25, 30, 40, 60,$ and 80 to converge the ICS for collision energies up to 0.3 eV. For details of the numerical parameters, please refer to the ESI.†

Fig. 1(A) shows the total reaction probabilities for the total angular momentum $J_{tot} = 0$ calculated using the 7D (with the CH bond length fixed in the original 8D model) and FT-6D models. The converged reaction probabilities rise rapidly as the collision energy increases from 0 to 0.2 eV without a reaction threshold, exhibiting many sharp and narrow oscillatory structures, especially for collision energies below 0.05 eV. Except at very low collision energies, the present reaction probabilities on the NN PES are larger than those[38,39] on the PWEM and vibronically and SO-coupled diabatic PESs. It can be seen that the 6D treatment can produce similar reaction probabilities to the 7D results, except that the 6D probabilities are slightly smaller between 0.02 and 0.15 eV. We, therefore, used the 6D model to carry out state-to-state calculations to reduce computational costs.

Fig. 1(B) shows the 6D HF vibrational state-resolved reaction probabilities as a function of collision energy. The $HF(v' = 2)$ state has the largest population in the entire energy region considered here, indicating an inverted HF vibrational state distribution. With increasing collision energy, the reaction probabilities for the $HF(v' = 1)$ state gradually increase, and the
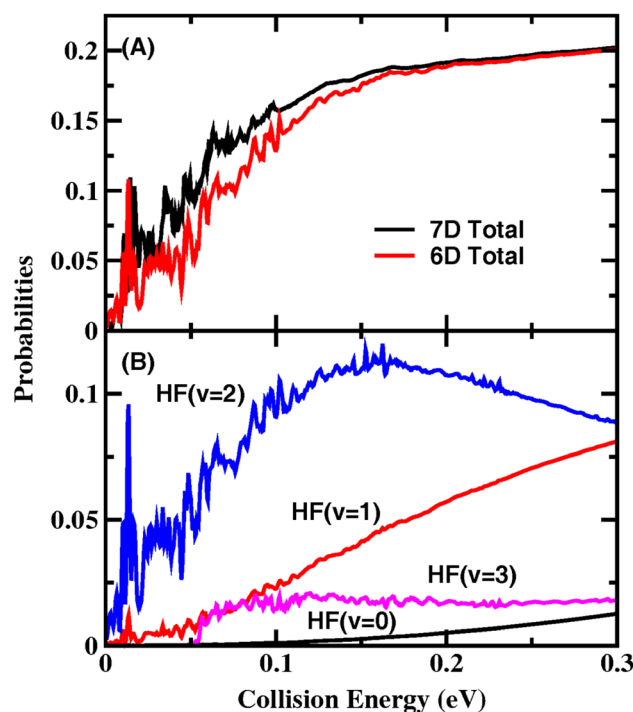

Fig. 1 (A) Total and (B) product HF vibrational state-resolved $J_{tot} = 0$ reaction probabilities for the initial ground rovibrational state as a function of collision energy.

fraction of HF($v' = 2$) decreases after 0.16 eV. The lowest vibrational state HF($v' = 0$) can only be observed at $E_c > 0.1$ eV as a smooth curve. The HF($v' = 3$) channel opens at a collision energy of 0.05 eV and has a probability that remains almost constant at high collision energies. The probabilities of the HF($v' = 1, 2, 3$) states all show oscillation peaks at low collision energies and become smooth in the high-energy region.

To investigate the dynamical origin of the oscillatory structures, we calculated the $J_{tot} = 0$ time-independent (TID) scattering wavefunctions at some collision energies for the reaction by performing Fourier transform of the time-dependent wavefunctions. Inspection of the two-dimensional contour of the wavefunction for the collision energy at 0.0135 eV in the product coordinates shown in Fig. 2(A) reveals that there exist three nodes along the H–F coordinate (correlating to the HF product) in the HF–CD$_3$ complex, but only two nodes for the outgoing wavefunction with a sudden decrease in amplitude. The sudden change in the nodal structure and amplitude of the wavefunction is the characteristic feature of a Feshbach resonance, indicating that the resonance is trapped in the HF($v' = 3$) VAP

well and produces mainly the HF($v' = 2$) product. Similar to the F + H$_2$/HD/HOD($v = 1$) reactions, the resonance wavefunctions of the title reaction are also narrow and located close to the barrier, and do not traverse the entire vdW well. The TID wavefunctions at the other low collision energies are found to have the same nodal structure as shown in Fig. 2(A).

To further confirm the mechanism of the resonance, we calculated the VAP for HF($v' = 0$–3) in the product region. The reaction coordinates are calculated in terms of $R_{F–CHD_3}$ on the reactant side and $R_{HF–CD_3}$ on the product side. As can be seen in Fig. 2(B), the VAP curves relevant to the vibrational states HF($v' = 0$–2) only have vdW wells. The minimum position of the vdW well moves from $R_{HF–CD_3} = 5.7 \, a_0$ for $v' = 0$, to 5.6 a_0 for $v' = 1$, and 5.4 a_0 for $v' = 2$, while the well depth increases slowly with v', from 0.082 eV for $v' = 0$, to 0.103 eV for $v' = 1$, and 0.137 for $v' = 2$. On the other hand, the HF($v' = 3$)–CD$_3$ VAP well is substantially deeper and is located much closer to the barrier than the HF($v' = 0$–2)–CD$_3$ vdW wells, which is the very peculiar well caused by chemical bond softening. The HF($v' = 3$)–CD$_3$ VAP has an asymptotic value of 0.0472 eV measured from the ground state of the reactants, and a well bottom lower than the ground state of the reactants. This means that the F + CHD$_3$ reaction can access the Feshbach resonances supported by the HF($v' = 3$)–CD$_3$ VAP well even with zero collision energy, which can only decay into lower HF($v' = 0$–2) vibrational states via vibrational predissociation before the HF($v' = 3$) channel opens. Therefore, the oscillating structures on the HF($v' = 1,2$) probabilities in Fig. 1(B) originate from the Feshbach resonance states trapped the peculiar HF($v' = 3$)–CD$_3$ VAP well created by the HF bond softening. The discernible oscillating structures on the HF($v' = 3$) probabilities and HF($v' = 2$) probabilities for $E_c > 0.05$ eV may originate from the bending excited HF($v' = 3$)–CD$_3$ VAP supported resonance states.

To investigate the effect of the resonance structures on the ICS, we calculated the ICS for the title reaction based on the reaction probabilities for $J_{tot} = 0, 10, 15, 20, 25, 30, 40, 60$ and 80, as shown in Fig. S1.† With increasing J_{tot}, the reaction probability curve shifts to higher energy, and the influence of the resonances on the reaction gradually fades. In order to take into account the change in the resonance structures with collision energy and J_{tot}, we estimated the reaction probabilities for partial waves $J_1 < J < J_2$ as

$$P^J(E) = P_{J_1}^J(E) \times f\cos(J) + P_{J_2}^J(E) \times [1 - f\cos(J)],$$

where

$$f\cos(J) = \frac{1}{2}\left[\cos\frac{\pi(J - J_1)}{J_1 - J_2} + 1\right],$$

$P_{J_1}^J(E) = P^{J_1}(E - \Delta E_1)$ and $P_{J_2}^J(E) = P^{J_2}(E + \Delta E_2)$ are obtained using the J-shifting approximation with $\Delta E_1 = [J(J + 1) - J_1(J_1 + 1)] \times B$, $\Delta E_2 = [J_2(J_2 + 1) - J(J + 1)] \times B$. B is a varying rotational constant for different $[J_1, J_2]$ intervals, which is obtained by minimizing the difference between $P^{J_1}(E - [J_2(J_2 + 1) - J_1(J_1 + 1)] \times B)$ and $P^{J_2}(E)$. Fig. 3(A) shows the HF vibrational state-resolved ICS as a function of collision energy. The shapes
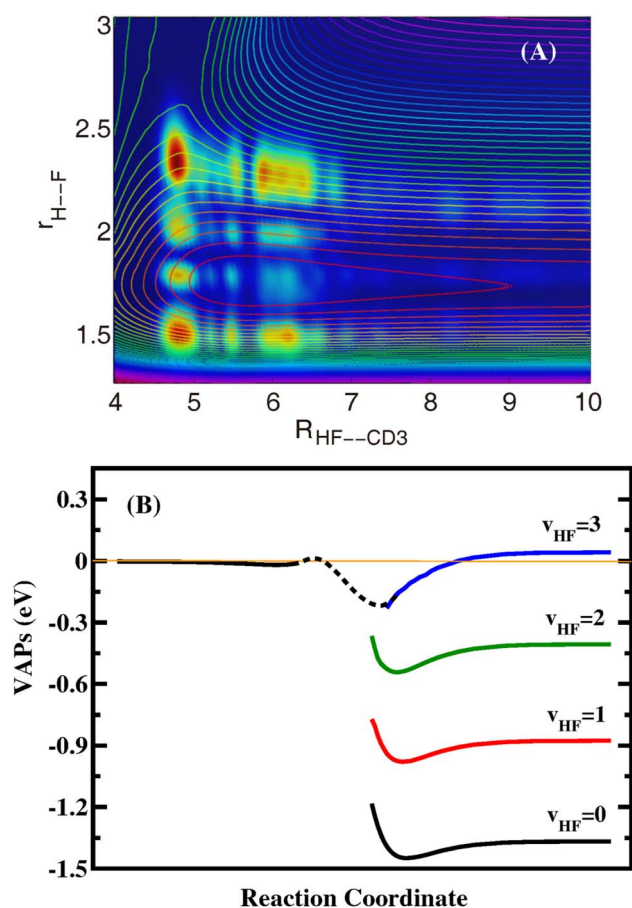

Fig. 2 (A) Reactive scattering wavefunctions for the title reaction in the two Jacobi coordinates R(HF–CD$_3$) and r(H–F) with other coordinates integrated at a collision energy of 0.0135 eV. The contour lines are the corresponding 2D PESs along the two reactive bonds R(HF–CD$_3$) and r(H–F) with the other coordinates optimized. (B) The calculated VAPs for the F + CHD$_3$ → HF + CD$_3$ reaction with different vibrational states of HF.
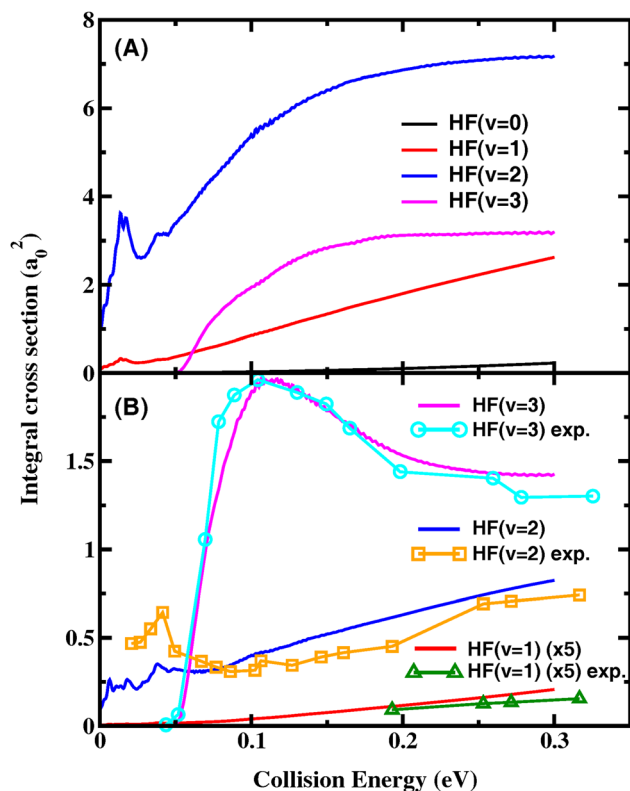
Fig. 3 Product HF vibrational state-resolved ICS for the title reaction as a function of collision energy (A) including all the rovibrational states of CD$_3$ and (B) for CD$_3$(v = 0) together with the experimental excitation functions in ref. 15.

of the excitation function are similar to the $J_{tot} = 0$ reaction probabilities in Fig. 1(B), except that the ICS of HF($v' = 3$) are higher than HF($v' = 1$) above $E_c = 0.062$ eV. Most resonance structures on the reaction probabilities vanish in the ICS after averaging over impact parameter J_{tot}, leaving only one distinct peak near $E_c = 0.015$ eV. In order to test the convergence of the ICS, four reaction probabilities ($J_{tot} = 10, 15, 25, 30$) were removed, and the cross-sections obtained using the $5 J_{tot}$ were in good agreement with those calculated with all 9 J_{tot}, even the resonance peaks, as shown in Fig. S2.† This proves that the J-shifting approximation method used here is reliable for reproducing the resonance structures on the reaction probabilities. Fig. S3† shows the normalized HF vibrational populations as a function of collision energy for the title reaction, which provide a comparison to the quasi-classical trajectories (QCT) results obtained using different methods on the CSBB PES.[45] It can be seen that the GB$_{ZPVE}$ method can reproduce the results near the threshold very well, while the GB$_{all}$ method is more suitable for higher energies.

Fig. 3(B) shows the HF vibrational state-resolved ICS for CD$_3$(v = 0) as a function of collision energy, along with the experimental excitation functions in ref. 15. The experimental and theoretical vibrational branching ratios of the product HF are in quantitative agreement with each other. The HF($v' = 2$) state is the sole contributor to the ICS in the low-energy regime. After the HF($v' = 3$) channel opens at $E_c = \sim 0.05$ eV, its ICS rises rapidly and

becomes the dominant channel. After reaching its peak at 0.1 eV, the HF($v' = 3$) ICS declines with further increase in the collision energy, causing the relative branching ratio of ($v' = 3$)/($v' = 2$) to decrease. Both the experimental and theoretical ICS of the HF($v' = 1$) state are very small throughout the entire energy region considered here. The experimental excitation functions of HF($v' = 2$) have a step-like feature near 0.04 eV as evidence of the resonance. Our theoretical ICS of the HF($v' = 2$) state shows a peak at about the same energy, but with a lower amplitude.

As can be seen, the theoretical ICS including all the rovibrational states of CD$_3$ shown in Fig. 3(A) are very different from those shown in Fig. 3(B) for the vibrational ground state of CD$_3$, indicating that the HF vibrational distributions strongly depend on the CD$_3$ umbrella states, or there exists a strong correlation between the vibrational distributions of the two product molecules. Fig. 4 shows the correlated ICS of the HF(v') + CD$_3$(v_2) product pair at collision energies of 0.0145 eV, 0.1 eV, 0.2 eV and 0.3 eV. The branching ratios are obtained by normalizing the CD$_3$ umbrella vibration distribution for each HF state at a given E_c. A strong anti-correlation between the vibration excitations of the paired products is apparent. At all four collision energies, as the HF excitation increases, the umbrella mode excitations of the correlated CD$_3$ show a noticeable decrease, and the proportion of CD$_3$($v_2 = 0$) becomes increasingly larger. The CD$_3$ umbrella state with the largest population changes from $v_2 = 6$ for $v' = 0$, to $v_2 = 4$ for $v' = 1$, to $v_2 = 3$ for $v' = 2$, and to $v_2 = 0$ for $v' = 3$. This strong anti-correlation between HF stretching and CD$_3$ umbrella motion is in agreement with what Liu and coworkers observed in the F + CD$_4$ reaction,[20–22] but the theoretical CD$_3$ umbrella mode excitations are much hotter than those observed in the F + CD$_4$ experiment, which were mainly populated in $v_2 = 0$–3. Because the umbrella angle of CD$_3$ in the transition state and that in the product are quite different for this early barrier reaction, strong vibrational excitation for umbrella motion is expected. The QCT-correlated ICS for HF(v') + CD$_3$(v_2) at a collision energy of 2.8 kcal mol^{-1} (0.121 eV) in ref. 45 showed the same anti-correlation trend, except that the present quantum mechanical (QM) CD$_3$ excitation is slightly hotter for HF($v' = 2$) and slightly colder for HF($v' = 3$), as shown in Fig. S4.†

Fig. S5† shows the correlated ICS of the HF(v') + CD$_3$(v_2) product pair, but the sum of the HF vibration populations for each CD$_3$ state at a given E_c is scaled to unity. For the ground CD$_3$ state, the HF vibration distribution is highly inverted, all peaking at $v' = 3$, except that the HF($v' = 3$) channel is energetically closed at $E_c = 0.0145$ eV. With higher umbrella excitation of CD$_3$, the vibration distribution of the correlated HF becomes colder, peaking at $v' = 2$ for $v_2 = 1$–6 and at $v' = 1$ for $v_2 = 7$–9 (for $E_c = 0.1$ eV), at $v' = 2$ for $v_2 = 2$–5 and at $v' = 1$ for $v_2 = 6$–9 (for $E_c = 0.2$ eV), and at $v' = 2$ for $v_2 = 1$–4 and at $v' = 1$ for $v_2 = 5$–9 (for $E_c = 0.3$ eV).

The anticorrelation of the HF(v') + CD$_3$(v_2) products in terms of the energy distribution is shown in Table S1 and S2.† At a fixed E_c, the average vibration energy of CD$_3$ ($\langle E_{v_2}\rangle_{CD_3}$) decreases with higher vibrational excitation of the correlated HF, while $\langle E_v\rangle_{HF}$ decreases when more energy is deposited into the umbrella mode of the CD$_3$ coproduct. Because the vibrational energy levels of HF are wide enough to offset the decrease in the correlated average vibration energy of CD$_3$, the sums of
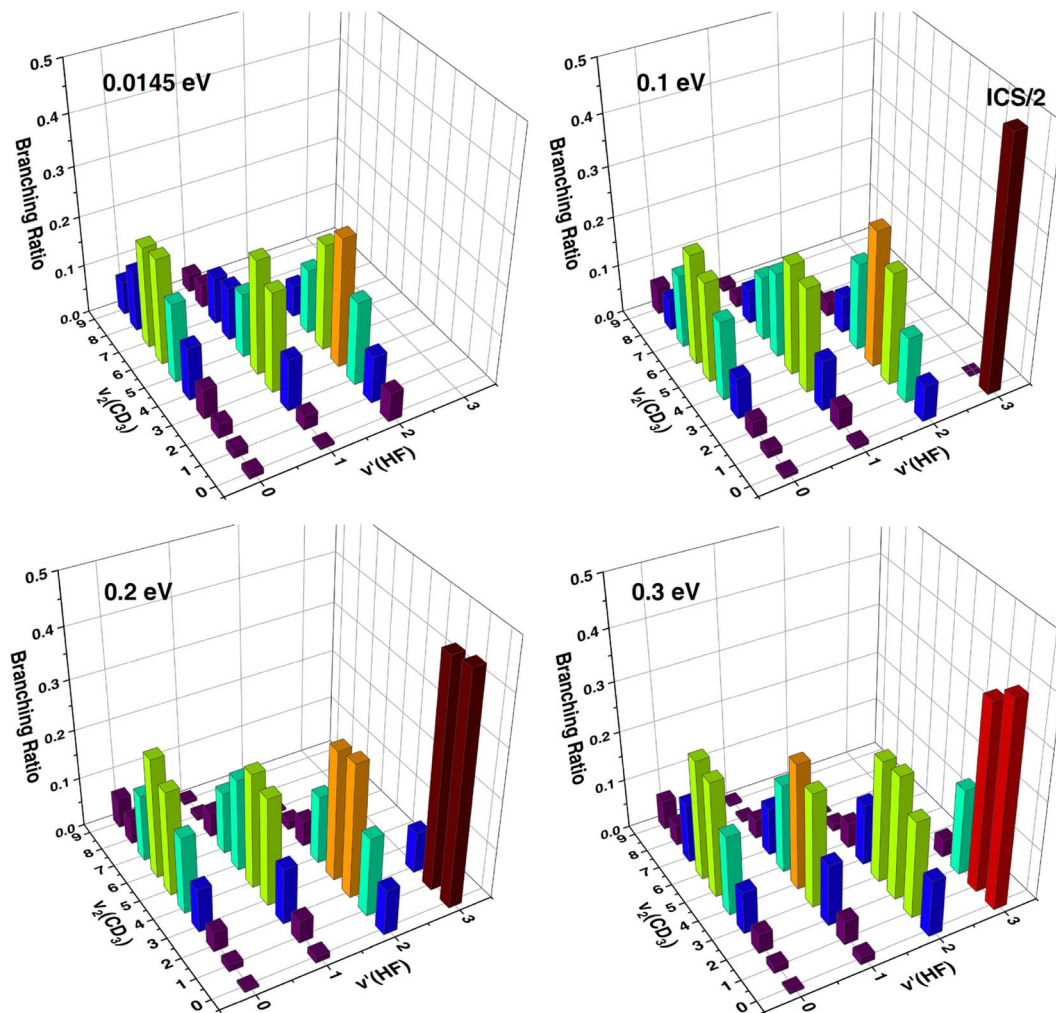
Fig. 4 Three-dimensional representation of the correlated ICS of the product pair of HF(v') and CD$_3$(v_2) at collision energies of 0.0145 eV, 0.1 eV, 0.2 eV and 0.3 eV; the sum of correlated CD$_3$ umbrella vibration populations for each HF state at a given E_c are scaled to unity.

$\langle E_{v_2} \rangle_{CD_3} + E_{HF}(v')$ increase with v'. On the other hand, the trend in $\langle E_v \rangle_{HF} + E_{CD_3}(v_2)$ is related to both v_2 and E_c.

Therefore, our quantum dynamics study of the F + CHD$_3$ → HF + CD$_3$ reaction on the highly accurate NN PES revealed that there exist pronounced oscillating structures in the total reaction probabilities, in particular in the low-collision-energy region, due to dynamical resonances trapped in the peculiar HF($v' = 3$) well in the post-barrier region, similar to those in the F + H$_2$/HD/H$_2$O/HOD reactions. Most of the resonance structures on the reaction probabilities are washed out in the ICS, leaving only a few oscillating structures in the ICS at low collision energies, in agreement with experimental observation. The theoretical HF vibrational state-resolved excitation functions for CD$_3$($v = 0$) agree very well with the experimental results, indicating that both the NN PES and quantum-dynamics method are sufficiently accurate for this reaction. A strong anti-correlated excitation of the two product vibrators HF(v') and CD$_3$(v_2) was found in the reaction, similar to what was observed experimentally, but the theoretical CD$_3$ umbrella vibration state distribution is much hotter than those observed in the F + CD$_4$ experiment.

Data availability

The data that support the findings of this study are available from the corresponding author upon request.

Author contributions

S. L. and D. H. Z. conceived the research and wrote the manuscript. S. L. performed the quantum dynamical calculation. J. C. and X. Z. developed the PES.

Conflicts of interest

There are no conflicts to declare.

Acknowledgements

References

1 M. Qiu, Z. Ren, L. Che, D. Dai, S. A. Harich, X. Wang, X. Yang, C. Xu, D. Xie, M. Gustafsson, R. T. Skodje, Z. Sun and D. H. Zhang, Observation of Feshbach resonances in the F + H2 → HF + H reaction, *Science*, 2006, **311**, 1440–1443.

2 Z. Ren, L. Che, M. Qiu, X. Wang, W. Dong, D. Dai, X. Wang, X. Yang, Z. Sun, B. Fu, S.-Y. Lee, X. Xu and D. H. Zhang, Probing the resonance potential in the F atom reaction with hydrogen deuteride with spectroscopic accuracy, *Proc. Natl. Acad. Sci. U. S. A.*, 2008, **105**, 12662–12666.

3 J. B. Kim, M. L. Weichman, T. F. Sjolander, D. M. Neumark, J. Kłos, M. H. Alexander and D. E. Manolopoulos, Spectroscopic observation of resonances in the F+H2 reaction, *Science*, 2015, **349**, 510–513.

4 T. Yang, L. Huang, C. Xiao, J. Chen, T. Wang, D. Dai, F. Lique, M. H. Alexander, Z. Sun, D. H. Zhang, X. Yang and D. M. Neumark, Enhanced reactivity of fluorine with para-hydrogen in cold interstellar clouds by resonance-induced quantum tunnelling, *Nat. Chem.*, 2019, **11**, 744–749.

5 T. Wang, J. Chen, T. Yang, C. Xiao, Z. Sun, L. Huang, D. Dai, X. Yang and D. H. Zhang, Dynamical resonances accessible only by reagent vibrational excitation in the F + HD → HF + D reaction, *Science*, 2013, **342**, 1499–1502.

6 R. Otto, J. Ma, A. W. Ray, J. S. Daluz, J. Li, H. Guo and R. E. Continetti, Imaging dynamics on the F + H2O → HF + OH potential energy surfaces from wells to barriers, *Science*, 2014, **343**, 396–399.

7 J. Ma and H. Guo, Reactive and nonreactive Feshbach resonances accessed by photodetachment of FH2O−, *J. Phys. Chem. Lett.*, 2015, **6**, 4822–4826.

8 X. Zhang, L. Li, J. Chen, S. Liu and D. H. Zhang, Feshbach resonances in the F + H2O → HF + OH reaction, *Nat. Commun.*, 2020, **11**, 223.

9 S. Liu, X. Zhang, J. Chen and D. H. Zhang, Feshbach resonances in the vibrationally excited F + HOD(vOH/vOD = 1) reaction due to chemical bond softening, *J. Phys. Chem. Lett.*, 2021, **12**, 6090–6094.

10 M. C. Babin, M. DeWitt, J. A. Lau, M. L. Weichman, J. B. Kim, H. Song, H. Guo and D. M. Neumark, Observation of resonances in the transition state region of the F+NH3 reaction using anion photoelectron spectroscopy, *Nat. Chem.*, 2023, **15**, 194–199.

11 N. Jonathan, C. M. Melliar-Smith and D. H. Slater, Initial vibrational energy distributions determined by infra-red chemiluminescence, *Mol. Phys.*, 1971, **20**, 93–102.

12 M. A. Nazar and J. C. Polanyi, Energy distribution among reaction products. XIV. F + CH4, F + CH3X(X = Cl, Br, I), F + CHnCl4−n(n = 1−3), *Chem. Phys.*, 1981, **55**, 299–311.

13 M. A. Wickramaaratchi, D. W. Setser, H. Hildebrandt, B. Körbitzer and H. Heydtmann, Evaluation of HF product distributions deduced from infrared chemiluminiscence. II. F atom reactions, *Chem. Phys.*, 1985, **94**, 109–129.

14 W. Shiu, J. J. Lin and K. Liu, Reactive resonance in a polyatomic reaction, *Phys. Rev. Lett.*, 2004, **92**, 103201.

15 J. Zhou, J. J. Lin and K. Liu, Observation of a reactive resonance in the integral cross section of a six-atom reaction: F + CHD3, *J. Chem. Phys.*, 2004, **121**, 813–818.

16 J. Zhou, J. J. Lin and K. Liu, Deciphering the nature of the reactive resonance in F + CHD3: correlated differential cross-sections of the two isotopic channels, *Mol. Phys.*, 2010, **108**, 957–968.

17 G. Czakó, Q. Shuai, K. Liu and J. M. Bowman, Experimental and theoretical investigations of the effects of the reactant bending excitations in the F+CHD3 reaction, *J. Chem. Phys.*, 2010, **133**, 131101.

18 R. T. Skodje, D. Skouteris, D. E. Manolopoulos, S.-H. Lee, F. Dong and K. Liu, Observation of a transition state resonance in the integral cross section of the F+HD reaction, *J. Chem. Phys.*, 2000, **112**, 4536.

19 F. Dong, S.-H. Lee and K. Liu, Reactive excitation functions for F+p-H2/n-H2/D2 and the vibrational branching for F+HD, *J. Chem. Phys.*, 2000, **113**, 3633.

20 J. J. Lin, J. Zhou, W. Shiu and K. Liu, State-specific correlation of coincident product pairs in the F + CD4 Reaction, *Science*, 2003, **300**, 966–969.

21 J. Zhou, J. J. Lin, W. Shiu and K. Liu, Insights into dynamics of the F+CD4 reaction via product pair correlation, *J. Chem. Phys.*, 2003, **119**, 4997.

22 J. Zhou, J. J. Lin, W. Shiu and K. Liu, State-correlation matrix of the product pair from F + CD4 → DF(v′) + CD3(0v200), *Phys. Chem. Chem. Phys.*, 2006, **8**, 3000–3006.

23 J. C. Corchado and J. Espinosa-García, Theoretical study of the CH4 + F → CH3 + FH reaction. I. Ab initio reaction path, *J. Chem. Phys.*, 1996, **105**, 3152.

24 D. Troya, Ab initio and direct quasiclassical-trajectory study of the F + CH4 → HF + CH3 reaction, *J. Chem. Phys.*, 2005, **123**, 214305.

25 C. Rángel, M. Navarrete and J. Espinosa-García, Potential energy surface for the F(2P3/2,2P1/2) + CH4 hydrogen abstraction reaction. Kinetics and dynamics study, *J. Phys. Chem. A*, 2005, **109**, 1441–1448.

26 J. Espinosa-García, J. L. Bravo and C. Rangel, New analytical potential energy surface for the F(2P)+CH4 hydrogen abstraction reaction: kinetics and dynamics, *J. Phys. Chem. A*, 2007, **111**, 2761–2771.

27 D. Troya, J. Millán and I. Baños, Ab initio potential energy surface, variational transition state theory, and quasiclassical trajectory studies of the F + CH4 → HF + CH3 reaction, *J. Chem. Phys.*, 2004, **120**, 5181.

28 J. F. Castillo, F. J. Aoiz, L. Bañares, E. Martinez-Nuñez, A. Fernández-Ramos and S. Vazquez, Quasiclassical trajectory study of the F + CH4 reaction dynamics on a Dual-level interpolated potential energy surface, *J. Phys. Chem. A*, 2005, **109**, 8459–8470.

29 G. Czakó, B. C. Shepler, B. J. Braams and J. M. Bowman, Accurate ab initio potential energy surface, dynamics, and thermochemistry of the F + CH4 → HF + CH3 reaction, *J. Chem. Phys.*, 2009, **130**, 084301.

30 G. Czakó and J. M. Bowman, An ab initio spin–orbit-corrected potential energy surface and dynamics for the F + CH4 and F + CHD3 reactions, *Phys. Chem. Chem. Phys.*, 2011, **13**, 8306–8312.

31 T. Westermann, W. Eisfeld and U. Manthe, Coupled potential energy surface for the F(2P) + CH4 → HF + CH3 entrance channel and quantum dynamics of the CH4 · F− photodetachment, *J. Chem. Phys.*, 2013, **139**, 014309.

32 T. Westermann, J. B. Kim, M. L. Weichman, C. Hock, T. I. Yacovitch, J. Palma, D. M. Neumark and U. Manthe, Resonances in the entrance channel of the elementary chemical reaction of fluorine and methane, *Angew. Chem., Int. Ed.*, 2014, **53**, 1122–1126.

33 T. Lenzen and U. Manthe, Vibronically and spin-orbit coupled diabatic potentials for X(P) + CH4 → HX + CH3 reactions: General theory and application for X(P) = F(2P), *J. Chem. Phys.*, 2019, **150**, 064102.

34 J. Chen, X. Xu, S. Liu and D. H. Zhang, A neural network potential energy surface for the F+CH4 reaction including multiple channels based on coupled cluster theory, *Phys. Chem. Chem. Phys.*, 2018, **20**, 9090.

35 G. Nyman and J. Espinosa-Garcia, Reduced dimensionality quantum scattering calculations on the F + CH4 → FH + CH3 reaction, *J. Phys. Chem. A*, 2007, **111**, 11943–11947.

36 D. Wang and G. Czakó, Quantum dynamics study of the F + CH4 → HF + CH3 reaction on an ab initio potential energy surface, *J. Phys. Chem. A*, 2013, **117**, 7124–7130.

37 H. F. von Horsten and D. C. Clary, Reactive resonances in the F+CHD3 reaction—a quantum dynamics study, *Phys. Chem. Chem. Phys.*, 2011, **13**, 4340–4356.

38 J. Qi, H. Song, M. Yang, J. Palma, U. Manthe and H. Guo, Mode specific quantum dynamics of the F + CHD3 → HF + CD3 reaction, *J. Chem. Phys.*, 2016, **144**, 171101.

39 B. Zhao and U. Manthe, Non-adiabatic transitions in the reaction of fluorine with methane, *J. Chem. Phys.*, 2020, **152**, 231102.

40 S. Liu, J. Chen, Z. Zhang and D. H. Zhang, A six-dimensional state-to-state quantum dynamics study of the H + CH4 → H2 + CH3 reaction (J = 0), *J. Chem. Phys.*, 2013, **138**, 011101.

41 J. Palma and D. C. Clary, A quantum model Hamiltonian to treat reactions of the type X + YCZ3 → XY + CZ3: Application to O(3P) + CH4 → OH + CH3, *J. Chem. Phys.*, 2000, **112**, 1859–1867.

42 M. T. Cvitaš and S. C. Althorpe, *J. Chem. Phys.*, 2011, **134**, 024309.

43 S. Liu, X. Xu and D. H. Zhang, Time-dependent wave packet theory for state-to-state differential cross sections of four-atom reactions in full dimensions: Application to the HD + OH → H2O + D reaction, *J. Chem. Phys.*, 2012, **136**, 144302.

44 Z. Zhao, S. Liu and D. H. Zhang, Differential cross sections for the H + D2O → HD + OD reaction: a full dimensional state-to-state quantum dynamics study, *Chin. J. Chem. Phys.*, 2017, **30**, 16–24.

45 G. Czakó and J. M. Bowman, Quasiclassical trajectory calculations of correlated product distributions for the F + CHD3 (v1 = 0,1) reactions using an ab initio potential energy surface, *J. Chem. Phys.*, 2009, **131**, 244302.